Spatial Distribution of RF-Induced E-Fields and Implant Heating in MRI

Peter Nordbeck,[1,2*] Florian Fidler,[2,3] Ingo Weiss,[4] Marcus Warmuth,[2] Michael T. Friedrich,[4] Philipp Ehses,[2] Wolfgang Geistert,[4] Oliver Ritter,[1] Peter M. Jakob,[2,3] Mark E. Ladd,[5] Harald H. Quick,[5] and Wolfgang R. Bauer[1]

The purpose of this study was to assess the distribution of RF-induced E-fields inside a gel-filled phantom of the human head and torso and compare the results with the RF-induced temperature rise at the tip of a straight conductive implant, specifically examining the dependence of the temperature rise on the position of the implant inside the gel. MRI experiments were performed in two different 1.5T MR systems of the same manufacturer. E-field distribution inside the liquid was assessed using a custom measurement system. The temperature rise at the implant tip was measured in various implant positions and orientations using fluoroptic thermometry. The results show that local E-field strength in the direction of the implant is a critical factor in RF-related tissue heating. The actual E-field distribution, which is dependent on phantom/body properties and the MR-system employed, must be considered when assessing the effects of RF power deposition in implant safety investigations.   Magn Reson Med 60:312–319, 2008. © 2008 Wiley-Liss, Inc.

Key words: electromagnetic fields; equipment safety; implants; magnetic resonance imaging; RF heating

MRI is one of the most powerful imaging modalities for a large number of clinical applications. Due to its excellent potential in soft tissue and functional imaging, millions of scans are performed every year with continuously increasing numbers. While MRI in general is considered to be a very safe imaging method, which rarely causes long-term side effects, there are in fact limitations regarding its usage in certain patient groups. A subject of strong interest is the question of whether medical implants containing magnetic and/or conducting components may be considered MR-safe. In a growing number of cases, patients with implanted electronic devices such as cardiac pacemakers, implantable cardioverter defibrillators (ICD), and neurostimulation systems like deep brain stimulators (DBS) are the focus of current investigations and controversial discussions.

A major problem regarding medical implants and patient safety in an MRI environment which is still unsolved is the tendency of elongated linear conductors to interact with the electric fields (E-fields) inherent to the MRI methodology. This particularly applies to guide wires and leads, such as those implanted with cardiac pacemakers, ICDs, as well as DBS implants. Inside the bore of an MR system these implants are especially vulnerable to picking up RF waves or electrical currents. This may lead to excessive heating with the capacity for severe tissue damage, especially at device-to-tissue interfaces that provide large differences in the electrical impedance and thus might locally concentrate RF energy, e.g., in the immediate vicinity of lead tips.

In phantom measurements, temperature increases near conductive wires of up to 48°C during MR scans have been reported (1). In vivo temperature measurements near implanted pacemaker leads in pigs revealed temperature increases of up to 20°C during MRI (2). A recently published case report of a patient with an implanted DBS who suffered serious permanent neurological injury due to a thermal lesion caused during MRI of the lumbar spine underlines that RF-related implant heating is a serious threat that must not be neglected (3).

On the other hand, there are simultaneously a growing number of reports on successful MRI in patients with implanted electrical devices without any discovered adverse outcomes. Some investigators have thus suggested that MRI in patients with cardiac pacemakers might be considered a diagnostic option as long as the imaging procedure rigidly conforms to carefully defined guidelines (4–6). All these investigations related to the safety of implanted electronic devices in an MRI setting are subject to ongoing controversial discussions that can be summarized with the statement "Failing to identify an adverse event is not equivalent to demonstrating safety" (7).

It has become clear that for MRI there is no safe-by-design implantable electronic device at this time, and unwanted side effects such as implant heating depend on a large variety of parameters (8–10). One parameter affecting the amount of tissue heating which still needs to be examined more carefully is the impact of the implant positioning inside the body. In vitro studies have shown that variances in configuration, positioning, and geometry of the device system result in large changes in the extent of heating (11,12), while factors allowing a concrete prediction of heating for particular positioning configurations remain unclear. Although calculations of localized power deposition inside the body during MRI have been recently

published, which to a certain degree refer to this question (13), that study did not focus on the impact of an implant's geometry inside the body on possible associated heating. RF-induced E-fields, which generate eddy currents in a conductive medium, are assumed to be responsible for the amount of implant heating during MR scanning (14,15). Meanwhile, the actual correlation between their appearance, magnitude, and implant heating is still unclear. Many studies investigating heating effects in MRI did not consider the impact of a large immersion medium such as the human body at all, but were performed with an experimental setup far different than a patient situation, i.e., in phantoms with limited extent and medium mass.

In this study, our main goal was to systematically investigate how variable implant positioning inside a given volume affects implant heating. A systematic investigation of correlations between the induced E-field distribution in large objects such as the human body and implant heating was the second goal of our study, aiming to help understand the complex and potentially harmful interactions between RF pulses and electric implants that occur inside the body during MRI.

MATERIALS AND METHODS

General Setup

All measurements were performed in an acrylic glass head/torso phantom according to the ASTM standard F2182-02a (16). The phantom was filled either with an aquatic saline solution or a viscous gel, both providing conductivity similar to that of body tissue as previously proposed (0.47 S/m) (18). Two methods were used to assess RF interactions in the phantom: E-field measurements with a custom probe and no implant in place, and temperature measurements near an elongated conductive rod. Both measurements were performed with systematically varying probe positioning inside the phantom medium to determine the 3D distribution of induced E-fields without the implant and the temperature induction near a linear conductive object. For the E-field measurements, phantom liquid consisted of 45 L of distilled water with 0.26% NaCl added. Heating measurements were performed in a semi-solid gel similar to those used by other groups before (17,18), made of 96.85% deionized water, 3% hydroxyethylcellulose, and 0.15% NaCl. Compared to gelled saline solutions relying on polyacrylic acid, this compound was found to be superior in terms of transparency, homogeneity, and long-term gel stability; prevention of convective heat transport was found to be comparable.

All MRI experiments were performed at 1.5T on two different MR scanners, a Siemens Magnetom Vision (hereafter referred to as Scanner 1) as well as a Siemens Magnetom Avanto (Scanner 2) (both Siemens Medical Solutions, Erlangen, Germany). The geometric center of the phantom torso filling was positioned exactly in the center of the scanner bore. The phantom was registered supine, head first, and the weight of the phantom was entered as 45 kg.

E-Field Measurements

A 3D map of MRI-related E-field distribution inside the phantom filling was sampled using a custom-made mea-surement system (Fig. 1). The E-field probe basically consists of a short dipole (50 mm in total) that drives a light-emitting diode (LED) (standard red, 10 mA) which converts the electric signal into light intensity. An optical fiber is used to transmit the light signal outside the scanner room, where it is converted by a phototransistor into an electrical signal, amplified (custom amplifier based on TL081CP, Texas Instruments, Dallas, TX), and finally measured with a digital multimeter (Fluke 87, Fluke Networks, Everett, WA). The optical link was chosen to avoid undesired induction of electrical signals in the connecting wires between the probe and the amplifier. A comparable technique has been used for measurements in liquid hyperthermia phantoms (19).

To increase the sensitivity of the sensor, a rectifier bridge (BAT43 diodes) was mounted in front of the LED. The LED does not pulse with the frequency of the RF signal, which is in the MHz range, but rather acts as a demodulator so that the envelope of the RF pulses is detected. This envelope correctly correlates to the pulse magnitude. The scanning sequence used consisted of regularly repeated pulses of equal magnitude; therefore, an adequate measure for the voltage intensity is the RMS value measured with the digital multimeter. The sensitivity of the sensor is frequency-dependent, and therefore the overall voltage response of the system must be calibrated for the desired working frequency if absolute measurements are of interest, e.g., using a dedicated workbench setup (20). For the scope of this study this was not required because only the E-field distribution was desired in terms of relative values that were obtained by normalizing the measurements to the maximum voltage gradient found for all positions and all orientations. Sensor characteristics in MRI were investigated prior to the measurements by variation of the RF power applied by the MR system.

In all, 1296 readings were performed in each scanner to assess the spatial distribution of RF-induced E-fields in the phantom filling. The dipole was systematically positioned at 432 measurement points distributed over three layers ($\frac{1}{4}$,
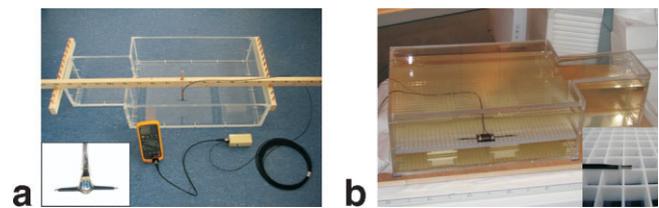

FIG. 1. **a:** Setup for E-field mapping during MRI inside a conductive medium, consisting of the sensor with integrated LED (close-up view) for electro-optical conversion, fiber optic cable, opto-electrical converter, and a digital multimeter. The wooden framework attached to the acrylic glass phantom was used to ensure precise and reasonably fast positioning of the sensor at the various measurement points (432 in total) and orientations (X, Y, and Z axes of the scanner bore) inside the saline. **b:** Experimental setup for measurement of RF-related heating at the tips of a straight steel rod inside gelled saline, showing one measurement point with the rod orientated in the Z-direction. Exact positioning of the rod inside the gel was ensured by the plastic frame and grid; the fiber optic temperature sensors were mounted at the tips of the rod and fixed with wax strings (close-up view).

1/2, and $\frac{3}{4}$ of saline filling height) inside the phantom filling with a wooden framework attached to the phantom. Three orthogonal orientations of the sensor were measured at each landmark, which were defined according to the three axes of the scanner bore as X (right to left), Y (dorsal to ventral) and Z, (head to feet). For each sensor configuration, one reading of RF-induced voltage gradient was performed while running a TrueFISP sequence with the acquisition parameters set as follows, identical for both MR systems: repetition time = 9.2 ms; echo time = 4.6 ms; flip angle = 60°; matrix = 256 × 256; field-of-view = 500 mm; slice thickness 10 mm; slices = 1; averages = 2; bandwidth = 130 Hz/pixel; acquisition time = 4.7 sec.

Temperature Measurements

Measurements of RF heating near an elongated conductive implant were performed using a 200 mm straight stainless steel rod of 1.5 mm diameter, both ends cut with flat faces. The steel rod was polyolefin-insulated (0.25 mm) apart from the first centimeter of both ends. Exact positioning of the rod inside the gel was ensured with the aid of a small plastic frame and a plastic grid in the phantom. For each steel rod position, temperature evolution near the rod was measured continuously during MRI with a fluoroptic temperature measurement system (Labkit m3300, Luxtron, Santa Clara, CA) and temperature sensors (STF-10, Luxtron) mounted at the rod tips (Fig. 1). Temperature increases were assessed in 180 geometric positions (X- or Z-direction, $\frac{1}{4}$, 1/2, and $\frac{3}{4}$ of gel filling height) by determination of mean temperatures in 10-sec intervals before and at the end of a specified MR scan, and subsequent computation of the difference.

A turbo spin-echo sequence with the following acquisition parameters for Scanner 1 (Scanner 2) was used: repetition time = 83.3 ms (97 ms); echo time = 15 ms (14 ms); turbo factor = 4 (7); flip angle = 82° (135°); matrix = 128 × 128 (512 × 512); field-of-view = 500 mm; slice thickness 10 mm; slices = 1; averages = 28 (14); acquisition time = 5:02 min. According to the system monitor, time averaged

power in Scanner 1 (Scanner 2) was 98.2–102.6 W (102.3 W), corresponding to a whole-body specific absorption rate (SAR) of 2.2–2.4 W/kg (2.2 W/kg).

RESULTS

E-Field Measurements

Preliminary testing of the E-field sensor revealed the sensor's local voltage pickup to increase monotonically with the indicated RF power output of a specific MR scanner for each position and orientation of the sensor in the phantom liquid. Dependency of the E-field sensor response on scanner power is shown for two representative setups in Fig. 2. All further measurements were performed with constant amplifier adjustments and constant sequence parameters. The spatial distribution and relative strength of locally induced E-fields in the phantom saline during MRI are summarized in Fig. 3 for Scanner 1 and in Fig. 4 for Scanner 2.

In both MR scanners, localized voltage gradients were in general strongest near the walls and weakest in the center of the phantom. Highest absolute values were found with the sensor orientated parallel to the long side of the phantom in proximity to the phantom wall (Z-direction). A right-left asymmetry in local E-field distribution (Z-component) was found in both scanners.

Temperature Measurements

Equivalent to the preliminary testing of the experimental setup for E-field measurements, preliminary testing of the RF heating experimental setup was performed with varying system power. RF heating near the conductive rod was found to be directly correlated to system power with a specific proportionality factor for each implant position and scanner type (Fig. 2).

A spatial distribution map of RF heating as a function of implant position was generated as described above; the results are condensed in Fig. 5. Maximum measured local gel heating at the implant tip was 26.8°C in Scanner 1 (rod
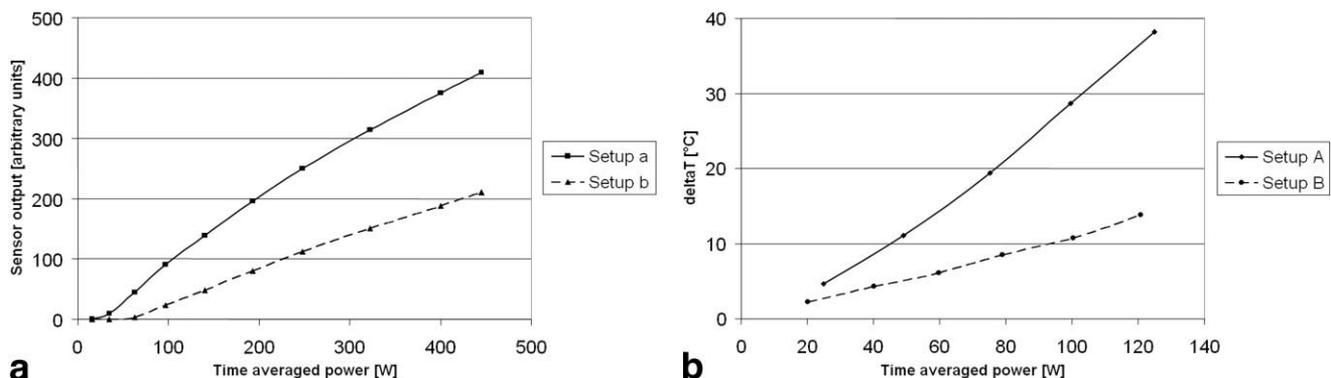
FIG. 2. **a:** MRI-related local voltage gradient dependent on scanner power. The normalized E-field sensor responses for two representative series of measurements in Scanner 1 are shown for the sensor at two different positions in the phantom saline. Time averaged power according to the system monitor was varied for each series by adapting the flip angle of the specified sequence; corresponding sensor output values are shown. **b:** Temperature increase near a conductive rod in Scanner 1 as a function of system power. Series of two representative setups (positions) are shown; time averaged power was adjusted by flip angle variation of the specified sequence. Note that in this study single point heating and E-field measurements in terms of numerical values cannot be directly correlated, mainly due to the different spatial resolutions achieved with both measurements.
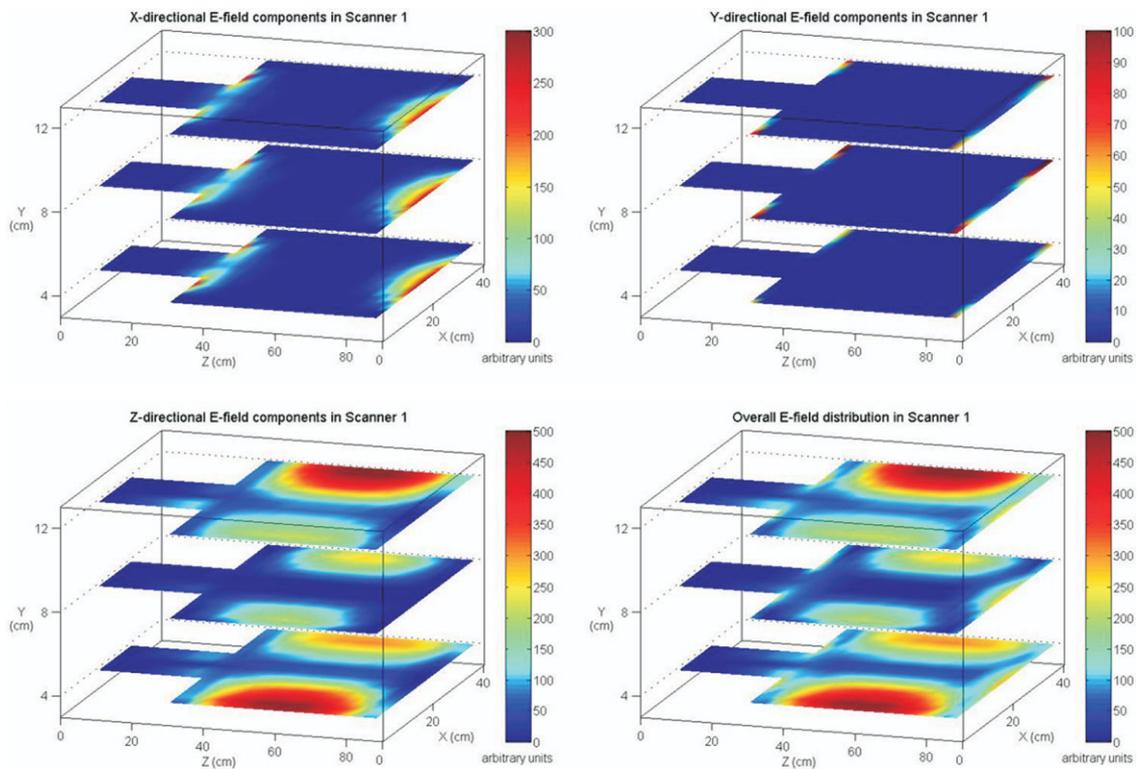
FIG. 3. Spatial distribution of induced E-fields within the phantom liquid in Scanner 1. Local voltage gradients were measured with the custom sensor as described; overall E-field distribution is assessed as $\sqrt{X^2 + Y^2 + Z^2}$. Arbitrary units represent sensor output values. Note different color scaling in the subfigures.
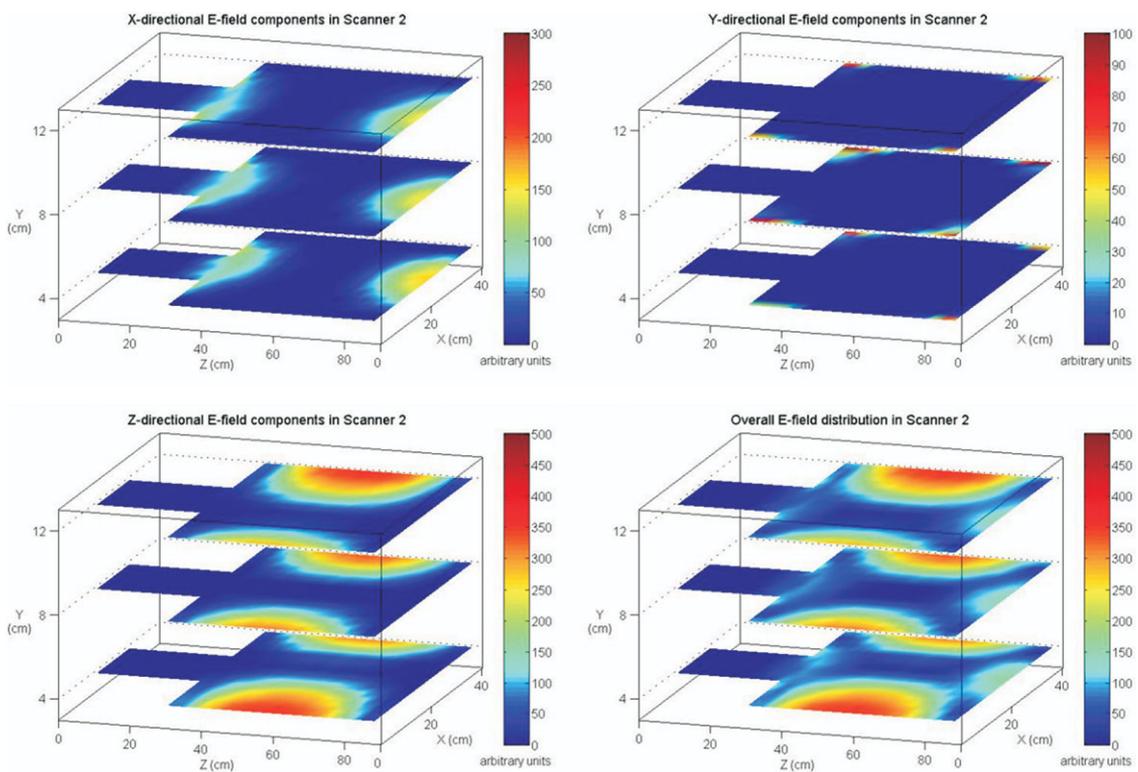

FIG. 4. Spatial distribution of induced E-fields within the phantom liquid in Scanner 2. Local voltage gradients were measured with the custom sensor as described; overall E-field distribution is assessed as $\sqrt{X^2 + Y^2 + Z^2}$. Arbitrary units represent sensor output values. Note different color scaling in the subfigures.
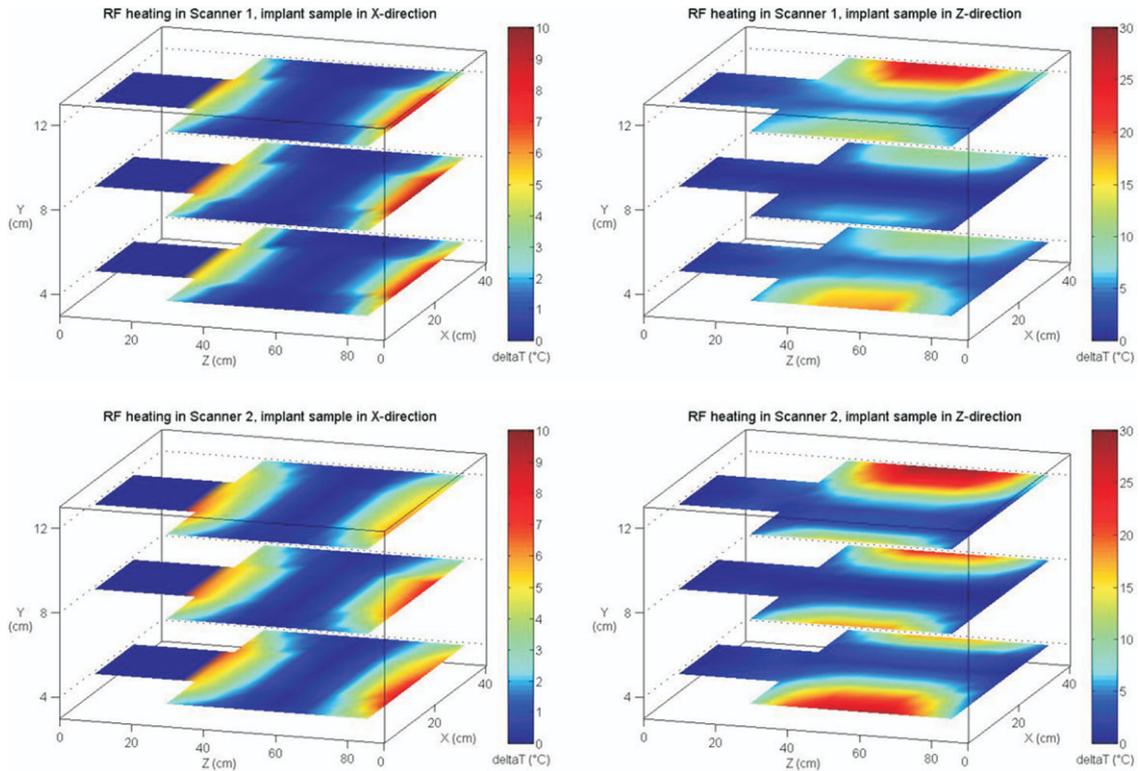
FIG. 5. Results of temperature measurements in both scanners, showing the local temperature increase at the tip of the rod orientated either in the X- or Z-direction during performance of the specified MR sequence. Each data point represents the temperature increase for a rod tip at that location with the other end of the rod oriented in the direction of the phantom midline, allowing temperature measurement across the full width and length of the phantom. Note that measurement of local RF heating in the head portion of the phantom was not possible in the X-direction due to the dimensions of the rod.
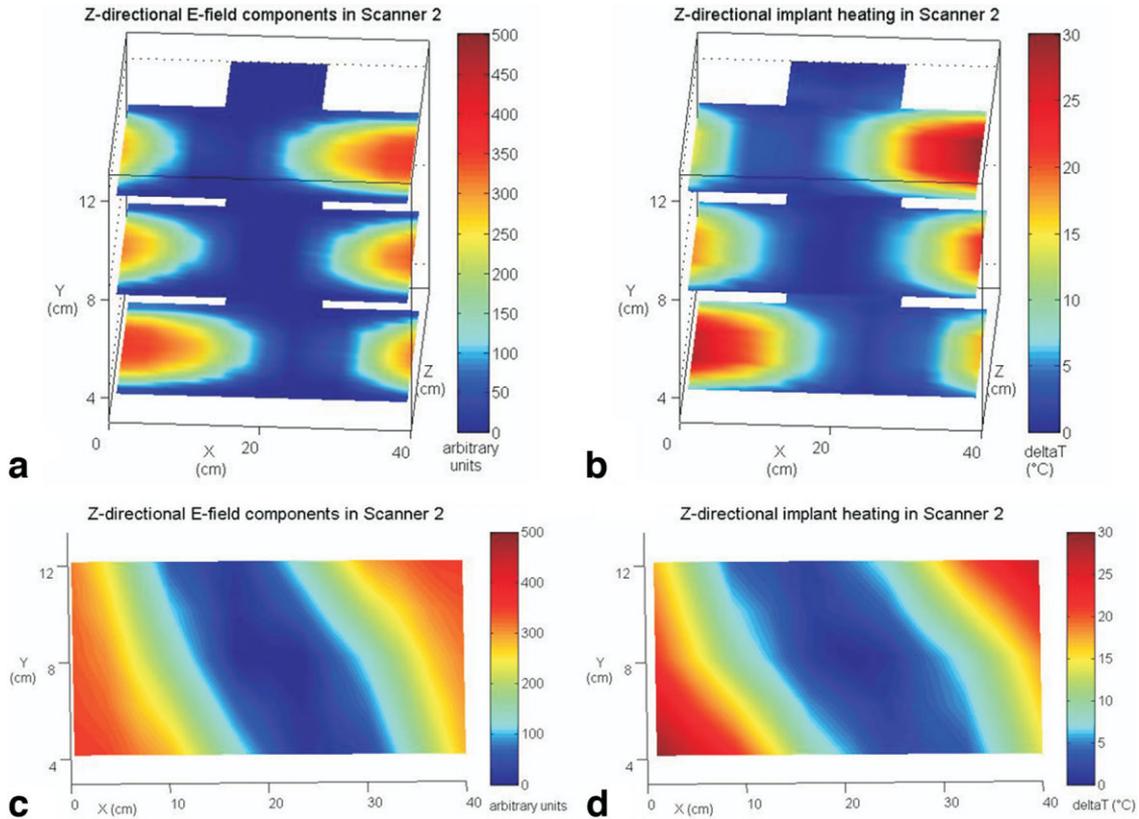
FIG. 6. Correlation of E-field and implant heating distribution in Scanner 2, showing three coronal (a,b) and a mid-torso transverse slice (c,d) of Z-directional measurements in the phantom. Left side (a,c): E-fields; right side (b,d): implant heating. Left-to-right asymmetry is apparent in both E-field and implant heating distributions, with the highest values at the upper left and lower right corner of the phantom. Scanner 1 qualitatively showed a comparable asymmetry in E-field and implant heating distribution.

along Z-direction in the top left corner) and 30.2°C in Scanner 2. In both scanners, minimum heating was found in the middle of the torso (0°C). Depending on implant position, the absolute value of RF heating in most cases differed between the two rod tips, with one tip developing an up to 2.2 times higher temperature increase than the other. This was especially the case for off-center positions of the rod, with one tip being closer to the phantom wall than the other, for both X- or Z-oriented rod positions. In positions with both tips symmetric to the phantom center, only minor differences between heating at both tips could be found. A right–left asymmetry in implant heating distribution (Z-orientation) was found in both scanners (Fig. 6).

DISCUSSION

The RF field of an MRI system is known to be capable of inducing excessive tissue heating, especially near elongated conductive leads and wires. Two mechanisms have been described that are held responsible for this undesirable effect in MRI. One is the electromagnetic induction heating, which may occur because RF can induce voltages in conductive media, ultimately causing circulating currents and ohmic heating (15,21). The other is the possible occurrence of resonating RF waves in the implant. This may lead to heating due to the so-called "Antenna Effect" (1,22). Standard guide wires containing stainless steel or alternatives without ferromagnetic components, like the nitinol-core Terumo device (1), and leads of electrical devices have been shown to be unsafe in the MR environment (2,3). These findings substantially contribute to the fact that under current guidelines the presence of an implanted cardiac pacemaker or ICD is considered to be a contraindication for routine MR imaging (23,24).

The aim of the present study was to systematically determine the distribution of RF-induced E-fields in a large object similar to the human body and to put these findings in the context of RF-related implant heating. Our findings show that implant heating only takes place if the implant follows the course of locally induced E-fields inside the conductive medium. Relative E-field strength was closely correlated to relative implant heating for corresponding landmarks inside the phantom medium (Fig. 6). The highest temperature increases were found if the implant was placed along the course of the highest voltage gradient distributions. No significant implant heating occurred if the implant was placed orthogonal to the local E-field course or in positions with very low overall E-field strength.

Pretesting of our dedicated E-field probe in MRI showed a monotonically increasing sensor response with ascending system power (Fig. 2). While the expected relationship according to theory would be a square root relation (20), we were not able to completely verify this relationship experimentally. This is probably due to additional factors such as the size of the E-field probe and possible nonlinearities of the diodes at low powers. An E-field sensor length of 50 mm was chosen as a compromise between sensitivity, measurement robustness, and spatial resolution while still avoiding major adverse effects regarding the accuracy of the E-field maps such as the occurrence of resonating RF waves in the probe (15,22).

The results of both E-field and temperature measurements show good congruence in terms of E-field distribution and RF heating map for the respective scanners. When putting the results of the study in context, though, it must be kept in mind that this investigation did not aim at—and thus does not allow for—an *exact conversion* of RF-related voltage gradients into temperature values induced near the implant tip at the respective position. The major reason why it is difficult to achieve such an approach in our measurements is the different length of E-field sensor and implant, preventing direct numerical comparisons without regard to E-field interferences along the whole implant length. The 50 mm length of the E-field sensor allowed for a total of 1296 readings without overlap of the measurement positions, while only 180 temperature measurement readings with the 200 mm implant were performed with partly overlapping rod positions. Thus, for example, the spatially limited high relative E-field strength near the head-torso intersection of the phantom, which is clearly shown in the E-field measurements, is not reflected in the temperature measurements. An implant length of 200 mm was chosen as a reasonable size for implants like cardiac pacemaker or DBS leads while being sufficiently short to allow for suitable positioning in the phantom to identify the "hot spots."

Our studies clearly show that different implant positions in a phantom or the human body—even with equal distances from the phantom wall and the scanner coil—do not necessarily lead to equivalent heating patterns, and specifics in local E-field distribution inside the medium are a crucial factor. This has to be considered when looking at the results of different studies focusing on heating effects in MRI, as different experimental setups (e.g., middle of the phantom vs. top left vs. top right corner) in our study led to a considerable difference in E-field strength and consequently implant heating. Moreover, nothing secure is known yet about how differing E-field distributions in different phantom configurations and especially in the inhomogeneous human body might influence the amount of RF heating. Because the induced in-phantom E-field or eddy currents are likely to be more apparent in a larger medium, it can be hypothesized that performing measurements in significantly smaller phantoms, as have often been used in previous studies for examining guide wire heating, increases the risk of underestimating possible RF heating in the human body.

RF-related power deposition as well as an approximate eddy current distribution inside a phantom filled with a conductive medium have been recently calculated (13). As a result, the eddy current distribution was predicted to have a circular characteristic along the outer walls of the body. Our experimental findings on both the distribution of induced E-fields as well as local implant heating show good agreement with these calculations. Local specific power deposition/SAR has been shown to be closely linked to the amount of induced implant heating. This is in line with our current findings, provided that an experimental setup was chosen where the implant was capable of picking up RF energy at all, which, for example, is not the case if the implant is orientated perpendicular to the local E-field direction. Local SAR alone without consideration of the E-field course is therefore an insufficient pa-

rameter to predict implant heating. Generally, we found the highest voltage gradients and temperature increases in places with the highest calculated power deposition in combination with a parallel orientation of implant or E-field sensor to the predicted eddy current direction, roughly following the phantom wall.

Two MRI systems were investigated to allow for a rough estimation of possible variances in E-field distribution and heating patterns between different MR scanners. We found a left-to-right asymmetry in E-field distribution as well as heating patterns in both scanners (Fig. 6), which is consistent with previously reported SAR calculations (13), and to some extent has been detected in other studies before (9). However, both E-field and implant heating measurements revealed that minor differences in E-field distribution and strength as well as local implant heating occur between the two scanner types. Most prominently, the E-fields as well as implant heating in Scanner 1 were concentrated closer to the head or feet walls of the phantom than in Scanner 2. Additionally, E-field strength and implant heating in the head section was generally more pronounced in Scanner 1. One possible explanation could be the design of the body coil, which differs at least in terms of coil length (1020 vs. 600 mm) and bore width (550 vs. 600 mm) between the scanners. While no fundamental qualitative differences between the two scanners were found in this study, variances might become more obvious when investigating other MRI systems with larger construction differences, especially in RF body coil design, as for example open bore MR scanners or systems with different field strengths.

The experimental results of our study again underline the findings of previous investigations on the question of MR safety of implanted electrical devices, showing that in certain cases even relatively small variances in an examination setup might lead to a major hazard and possible adverse outcomes. While up to the present date numerous MR investigations on patients with implanted electronic devices have been performed without any recognized adverse outcome (5,6,25), on the other hand catastrophic incidents have been reported (3,26). We could show in the phantom environment that under certain conditions a simple reorientation of the implant led to either virtually no heating at all or up to a 30°C temperature increase, even though the implant tip remained in the same position. Moreover, the marked left-to-right asymmetry shows that extending conclusions from one tested setup of an implanted device to another is problematic unless the E-field distribution in the body has been very carefully investigated for a specific MR system and setup. While our study confirms again that heating is in fact linearly related to SAR/system power, we could clearly show that this is just one proportionality factor among others. Therefore, absolute proposals of "safe" SAR limits—or even flip angles—as proposed, for example, for DBS systems (8), are problematic in our opinion, as long as other specific properties of the medium, device, and MR scanner, which all contribute to this issue, remain unclear. This stresses the importance of developing MR-compatible devices that are inherently safe by design rather than scanning conventional implanted devices in an MRI surrounding under "controlled conditions" that might just be "safe by chance."

All measurements in the present study were performed in a standardized phantom, roughly providing conditions in terms of size and conductivity similar to those in the human body. The E-field distribution and the implant heating map might therefore allow for a rough prediction of "high risk" device setups in the human body. It has to be noted, however, that depending on body tissue distribution, major differences in the RF-related E-field distribution in a patient with an implanted electrical device must be expected, thus making it hard to absolutely predict possible implant heating in vivo.

CONCLUSION

As another step toward understanding the mechanisms of RF implant heating in MRI, the present study provides a systematic investigation of the impact of implant positioning inside a human body-like phantom on RF-induced tissue heating near the tip of an elongated conductive implant. The E-field distribution without an implant and the "hot spots" with an inserted implant inside a phantom torso were experimentally assessed at 1.5T in two different MR scanners. It was possible to predict implant heating by measurement of E-field components in the medium. A specific hazard for excessive tissue heating during MRI arises if elongated conductive implants follow the course of the RF-related E-field in the body. No significant implant heating occurs in positions with low overall E-field strength or if the implant is positioned orthogonal to the local E-field; local SAR alone without consideration of the local E-field course is therefore an insufficient parameter to predict implant heating. As implant heating depends on the actual E-field distribution in the medium, in vitro investigations on MR-related implant heating should be performed in an experimental setting providing conditions, including phantom size, similar to the human body.

REFERENCES

1. Konings MK, Bartels LW, Smits HF, Bakker CJ. Heating around intravascular guidewires by resonating RF waves. J Magn Reson Imaging 2000;12:79–85.
2. Luechinger R, Zeijlemaker VA, Pedersen EM, Mortensen P, Falk E, Duru F, Candinas R, Boesiger P. In vivo heating of pacemaker leads during magnetic resonance imaging. Eur Heart J 2005;26:376–383.
3. Henderson JM, Tkach J, Phillips M, Baker K, Shellock M, Rezai AR. Permanent neurological deficit related to magnetic resonance imaging in a patient with implanted deep brain stimulation electrodes for parkinson's disease: case report. Neurosurgery 2005;57:1063–1066.
4. Martin ET, Coman JA, Shellock FG, Pulling CC, Fair R, Jenkins K. Magnetic resonance imaging and cardiac pacemaker safety at 1.5-Tesla. J Am Coll Cardiol 2004;43:1315–1324.
5. Roguin A, Zviman MM, Meininger GR, Rodrigues ER, Dickfeld TM, Bluemke DA, Lardo A, Berger RD, Calkins H, Halperin HR. Modern pacemaker and implantable cardioverter/defibrillator systems can be magnetic resonance imaging safe: in vitro and in vivo assessment of safety and function at 1.5 T. Circulation 2004;110:475–482.
6. Sommer T, Naehle CP, Yang A, Zeijlemaker V, Hackenbroch M, Schmiedel A, Meyer C, Strach K, Skowasch D, Vahlhaus C, Litt H, Schild H. Strategy for safe performance of extrathoracic magnetic resonance imaging at 1.5 Tesla in the presence of cardiac pacemakers in non-pacemaker-dependent patients: a prospective study with 115 examinations. Circulation 2006;114:1285–1292.

7. Gimbel JR, Kanal E. Can patients with implantable pacemakers safely undergo magnetic resonance imaging? J Am Coll Cardiol 2004;43:1325–1327.

8. Finelli DA, Rezai AR, Ruggieri PM, Tkach JA, Nyenhuis JA, Hrdlicka G, Sharan A, Gonzalez-Martinez J, Stypulkowiski PH, Shellock FG. MR Imaging-related heating of deep brain stimulation electrodes: in vitro study. AJNR 2002;23:1795–1802.

9. Baker KB, Tkach JA, Nyenhuis JA, Phillips M, Shellock FG, Gonzalez-Martinez J, Rezai AR. Evaluation of specific absorption rate as a dosimeter of MRI-related implant heating. J Magn Reson Imaging 2004;20:315–320.

10. Nitz WR, Brinker G, Diehl D, Frese G. Specific absorption rate as a poor indicator of magnetic resonance-related implant heating. Invest Radiol 2005;40:773–776.

11. Baker KB, Tkach JA, Hall JD, Nyenhuis JA, Shellock FG, Rezai AR. Reduction of magnetic resonance imaging-related heating in deep brain stimulation leads using a lead management device. Neurosurgery 2005;57:392–397.

12. Sommer T, Valhaus C, Lauck G, Smekal A, Reinke M, Hofer U, Block W, Träber F, Schneider C, Gieseke J, Jung W, Schild H. MR imaging and cardiac pacemakers: in vitro evaluation and in vivo studies in 51 patients at 0.5 T. Radiology 2000;215:869–879.

13. Amjad A, Kamondetdacha R, Kildishev AV, Park SM, Nyenhuis JA. Power deposition inside a phantom for testing of MRI heating. IEEE Trans Magn 2005;41:4187–4187.

14. Armenean C, Perrin E, Armenean M, Beuf O, Pilleul F, Saint-Jalmes H. RF-induced temperature elevation along metallic wires in clinical magnetic resonance imaging: influence of diameter and length. Magn Reson Med 2004;52:1200–1206.

15. Dempsey MF, Condon B, Hadley DM. Investigation of the factors responsible for burns during MRI. J Magn Reson Imaging 2001;13:627–631.

16. American Society for Testing and Materials. Standard test method for measurement of radio frequency induced heating near passive implants during magnetic resonance imaging (F2182–02a). West Conshohocken, PA: ASTM International; 2002.

17. Shellock F, Valencerina S. Septal repair implants: evaluation of magnetic resonance imaging safety at 3 T. Magn Reson Imaging 2005;23:1021–1025.

18. U.S. Food and Drug Administration. SAR intercomparison protocol for MR systems. Draft Oct 2005.

19. Schneider CJ, Engelberts N, van Dijk JDP. Characteristics of a passive RF field probe with fibre-optic link for measurements in liquid hyperthermia phantoms. Phys Med Biol 1991;36:461–474.

20. Taylor HC, Burl M, Hand JW. Design and calibration of electric field probes in the range 10-120 MHz. Phys Med Biol 1997;42:1387–1394.

21. Yeung CJ, Susil RC, Atalar E. RF heating due to conductive wires during MRI depends on the phase distribution of the transmit field. Magn Reson Med 2002;48:1096–1098.

22. Ladd ME, Quick HH. Reduction of resonant RF heating in intravascular catheters using coaxial chokes. Magn Reson Med 2000;43:615–619.

23. Kanal E, Borgstede J, Barkovich AJ, Bell C, Bradley WG, Etheridge S, Felmlee JP, Froelich JW, Hayden J, Kaminski EM, Lester JW, Scoumis EA, Zaremba LA, Zinninger AM. American College of Radiology White Paper on MR Safety. AJR Am J Roentgenol 2004;182:1111–1114.

24. Faris OP, Shein M. Food and Drug Administration perspective: magnetic resonance imaging of pacemaker and implantable cardioverter-defibrillator patients. Circulation 2006;114:1232–1233.

25. Gimbel JR, Wilkoff BL, Kanal E, Rozner MA. Safe, sensible, sagacious: responsible scanning of pacemaker patients. Eur Heart J 2005;26:1683–1684.

26. Rezai AR, Baker KB, Tkach JA, Phillips M, Hrdlicka G, Sharan AD, Nyenhuis J, Ruggieri P, Shellock FG, Henderson J. Is magnetic resonance imaging safe for patients with neurostimulation systems used for deep brain stimulation? Neurosurgery 2005;57:1056–1062.